Iranian Journal of Materials Forming 10 (1) (2023) 61-69

Online ISSN: 2383-0042

IJMF

Iranian Journal of Materials Forming

Journal Homepage: http://ijmf.shirazu.ac.ir

Research Article

On the Substructure Development and Continuous Recrystallization in the Course of Selective Laser Melting of 316L Stainless Steel

Z. Abbasi and H.R. Abedi*

School of Metallurgy & Materials Engineering, Iran University of Science and Technology (IUST), Tehran, Iran

ARTICLE INFO

Article history:

Received 17 March 2023
Reviewed 17 April 2023
Revised 3 May 2023
Accepted 14 May 2023

Keywords:

Stainless steel
Selective laser melting (SLM)
Cellular structure
Recrystallization
Recovery

Please cite this article as:

Z. Abbasi, H.R. Abedi, On the substructure development and continuous recrystallization in the course of selective laser melting of 316L stainless steel, *Iranian Journal of Materials Forming*, 10(1) (2023) 61-69.

ABSTRACT

In the present work, the selective laser melting (SLM) has been chosen as a controlled thermomechanical processing route in which the required temperature and strain for the occurrence of dynamic recrystallization is provided. The 316L stainless steel as representative material was constructed by SLM under specified parameters (laser power, layer thickness, hatch spacing, scan strategy, and scan speed). The printed material's microstructure was carefully analyzed through electron back scattered diffraction. The presence of considerable fine grains (< 20 μm) through the printed microstructure was considered as evidence for the occurrence of dynamic recrystallization during the manufacturing process. The high fraction of sub-boundaries (~79.7%) and sub-grains indicated the capability of the material for substructure development in the course of additive manufacturing process, and the fact that the new fine grains were formed through continuous dynamic recrystallization mechanism. The creation of plastic strains through the parts structure during SLM, which was required for dynamic recrystallization, was discussed relying on the expansion and contraction of the layers during repeated heating and cooling cycles. The amount of plastic microstrain was estimated to be around ~0.56 considering the layer thickness and depth of the melt pool. The hot compression tests were conducted at 1000°C and various strain rates of 0.001, 0.01 and 0.1 s^{-1} and the corresponding critical strains of dynamic recrystallization (~0.2) were calculated, which was well lower than those created during additive manufacturing process.

1. Introduction

The additive manufacturing of the components has drawn much attention owing to their high potential for layer-by-layer production of intricate details with excellent dimensional accuracy from metals, ceramics, polymers, and composites [1]. Due to the component's close-resemblance to its final shape, and processing steps, the required consumables, production and assembly costs, and time are considerably reduced [2-5]. The mechanical and functional properties of the fabricated components are comparable with those made using conventional production techniques such as casting and forging [6]. However, the differences in structural defects, residual stress, and anisotropy should be considered thereby [7]. In the case of SLM as a

* Corresponding author
E-mail address: habedi@iust.ac.ir (H.R. Abedi)
https://doi.org/10.22099/IJMF.2023.47020.1255

powder bed fusion process, the low-thickness powder is sprinkled on the substrate and melted by applying a high-power laser, and this cycle will be continued with layer-by-layer freezing until the final shape is achieved [8]. The SLM method typically experiences an ultra-high cooling rate, where the production program is controllable based on the settings in each layer for the scan speed, beam size (and energy density), scan distance, and scanning strategy. The change in these parameters will lead to a change in the microstructural characteristics in respect of the grain size, deposits, and texture [9]. These characteristics are fundamentally connected to the unique mechanical and functional properties of the printed products. The results of most of the research indicate that the materials produced by additive manufacturing methods have unique structural characteristics and their functional/mechanical properties are entirely comparable to (and higher than) those produced through conventional production methods.

In respect of the probable grain refinement which may occur in the course of selective laser melting, some studies developed numerical models to predict the grain structure during the laser powder bed fusion (LPBF) process [10, 11]. These are mainly based on the cellular automata (CA) combined with a model which considers the thermal fields and thermal histories that control the grain growth [12-15]. In line with these efforts, Bertsch et al. [16] have experimentally examined the origin of dislocation-substructures in selective laser-melted 316L stainless steel by fabricating "1D-rods", "2D-walls", and "3D-prisms". They systematically indicated that the formation of dislocation cell structure is correlated with thermal distortions in the course of printing. Constraints surrounding the melt pools and thermal cycling are known as the main causes of distortion. The present authors believed that the substructure developed during selective laser melting may be accompanied by the occurrence of either the dynamic or post-dynamic recrystallization.

The occurrence of grain refinement during post-heat treatment or by controlling the cooling rate of the additive manufacturing process has been extensively examined [17-20], however, to the best of authors' knowledge, the formation possibility of fine recrystallized grains during SLM has been mainly overlooked in previous research. To this end, the present piece of research has focused on the probability and how the restoration processes (recrystallization and recovery) occur during SLM of 316L stainless steel (as representative material), which can significantly affect the subsequent mechanical properties. We deal with selective laser melting as a thermomechanical processing route in which the required temperature and strain for the occurrence of dynamic recrystallization are provided. The outcomes are expected to increase the knowledge regarding the microstructure-controlled based additive manufacturing of stainless steels.

2. Experimental Procedure

2.1. Selective laser melting (SLM)

The cylindrical samples of 316L stainless steel the size 8 mm in diameter and 12 mm in height were produced through the SLM technique. Table 1 shows the powder's chemical composition utilized for printing.

Table 1. Powder's chemical composition used in the selective laser melting of 316L alloy (wt.%)

Fe	Cr	Ni	Mo	Mn	Si	P	C
67.9	17.13	11.1	2.4	1.4	0.45	0.029	0.03

The powder comprises spherical particles with an average size of about 45 µm. The samples were printed by the Noura M100 machine in Noura company. The chamber was controlled by argon gas, and the process variables are given in Table 2. During the manufacturing process, 402 layers of powder were melted for 7 h, and 120 g of desired metal powder were consumed. Each layer's laser scanning direction was 90° rotated from the previous.

Table 2. Manufacturing parameters of the piece during selective laser melting

Laser power	Thickness	Hatch space	Scan speed
300 W	30 µm	75 µm	750 mm s^{-1}

2.2. Hot compression

In order to determine the required critical strain for the initiation of dynamic recrystallization, the selective laser melted material has been deformed in compressive mode at 1000°C under strain rates of 0.1 s^{-1}, 0.01 s^{-1}, and 0.001 s^{-1}. The employed servomechanical universal testing machine was equipped with a split furnace with the temperature accuracy of ±2°C and an interface load-cell with the load accuracy of 0.1 kg. The specimens were held for 7 min to reach the equilibrium condition and then compressed down to the true strain of 0.6. Mica sheets were utilized to minimize the friction effect between surface and anvils. The corresponding true stress-true strain curves were extracted and analyzed to shed light on the recrystallization characteristics of the experimented alloy.

2.3. Microstructure investigation

The selective laser melted component was prepared through standard metallographic methods and the corresponding microstructure was carefully studied with the help of a scanning electron microscope equipped with electron back-scattered diffraction. To explore the probability of dynamic recrystallization during laser melting, the grain size distribution developed substructure (sub-boundaries sub-grains), as well as the micro-texture were investigated. The direction of making the piece and the scanning direction are in the Y and the X direction, respectively.

3. Results and Discussion

Fig. 1(a) displays the inverse pole figure map of the 316L sample created by the selective laser melting process. The as-processed structure is composed of a single austenite phase in which the grains and melt pools are discernible. For the construction of the inverse pole figure, the Y axis corresponds to the construction direction and has been considered as the reference axis.

The 316L-SLM possesses a hierarchical structure including a melt pool, grain, and cellular substructure [21, 22]. In the present case, the microstructure is composed

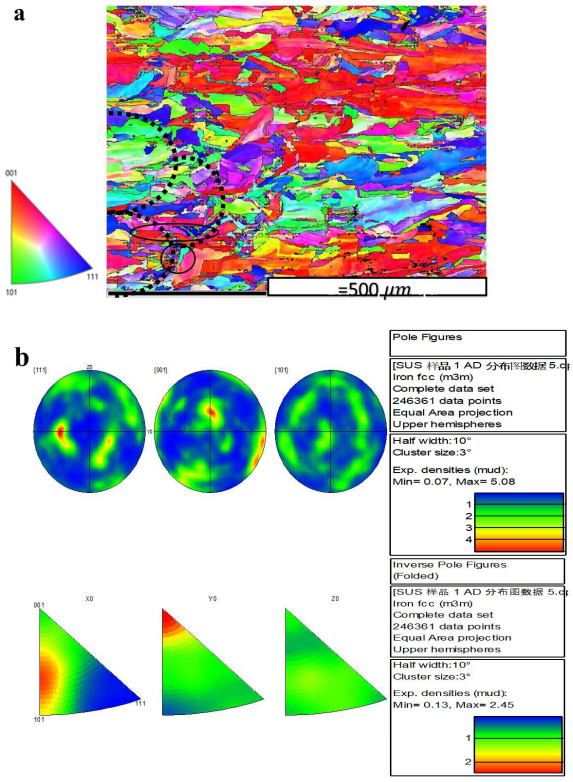

c

Grain size (μm)	Percent (%)
3.45	0.1%
4.53	0.2%
5.94	0.7%
7.79	0.9%
10.22	0.9%
13.4	2.3%
17.57	2.7%
23.04	4.4%
30.21	8.4%
39.62	6.9%
51.95	4%
68.12	15.6%
89.33	37.1%
117.13	15%

Fig. 1. (a) Inverse pole figure of the processed structure of 316L steel through selective laser melting. The buliding direction (Y) has been considered as reference axis, (b) pole figures of (001), (011), and (111) planes besides the inverse pole figures with different reference axes of X, Y, and Z, (c) the corresponding grain size distribution of printed microstructure.

composed of elongated dendrites at the melting pool center and equiaxed ones at the melting pool boundary. The main reason for such cellular/dendritic growth patterns is the thermal history experienced by each region. The solidified microstructure consists of grains (elongated or equiaxed). The very rapid cooling rate (10^6-10^8 K/s) of the SLM process, specified heat distribution gradient, and directional freezing have been introduced as the main cause of this specified growth pattern [23, 24]. The temperature gradient (G), growth

rate (R), and solidification undercooling (ΔT) in a melt pool vary considerably from one local region to another and, therefore, the microstructure varies. The effect of thermal gradients on the solidification structure, which is described by undercooling criterion, can be mathematically stated by equations below:

$$\frac{G}{R} > \frac{\Delta T}{D_1} \quad (1)$$

$$\frac{G}{R} < \frac{\Delta T}{D_2} \quad (2)$$

The first equation represents the condition for the formation of columnar grains and the second is for equiaxed grains where D is the diffusion coefficient. While G/R ratio controls the solidification microstructure, the cooling rate in terms of $G \times R$ determines the fineness of the structure in a sense that the higher the product, the finer the structure [25]. Fig. 1(c) shows the grain size distribution of printed microstructure, where the grain size ranges between 1 to 130 μm. Despite the elongation of the grains and a high fraction of the grains which are above 50 μm, but still a significant part of the grains is below 20 μm, indicating the experience of a dynamic recrystallization during the part-making process. The average grain size of the printed microstructure is 73.3 μm owing to the high portion of the grains in the size of ~89 μm, which is about 37% of all grains. However, it shows that about 8% of the grains possess the size under 20 μm, especially in melt pool boundary.

A considerable portion of the structure consists of grains holding <001> orientation. This has also been observed in previous studies [26] and has been attributed to the epitaxial growth of the pools during solidification and the rotating scanning strategy selected during the process. Owing to the directional solidification and the specified heat distribution/transfer in the course of selective laser layer-by-layer melting, the grains are characterized as elongated in the direction of the molten pools and perpendicular to the building direction holding a width of fewer than 100 μm. The width of the grains in the structure is attributed to the super-cooling factors and the temperature gradient during the solidification of the melt pool. It is important to point out that some small equiaxed grains can be also traced besides the elongated grains, which may signify the occurrence of dynamic recrystallization during the manufacturing process or post-dynamic recrystallization occurring in the course of subsequent cooling.

For a detailed investigation of the orientation and local texture of the developed grains, pole figures of (001), (011), and (111) planes and inverse pole figures holding different reference axes are shown in Fig. 1(b). Multiple (001) poles with the highest intensities are characterized as dominant microtextures which have been oriented perpendicular or parallel to the direction of construction. In addition, the intensities of (111) poles along the building direction and also (110) poles 45°-oriented toward the building direction should be considered.

The presence of fine and equiaxial grains through the microstructure indicates the material has experienced the restoration phenomena during the manufacturing process the selective laser melting can be considered as a controlled thermomechanical processing route. According to the high angle grain boundary map of the SLMed structure in Fig. 2(a), the volume fraction of recrystallized grains (fine and equiaxed) is considerable. Examining the low angle boundaries map in Fig. 2(b) and Fig. 2(c) indicates the high capability of the experimented material for the development of substructure and low-angle boundaries formation in the course of selective laser melting.

In Fig. 2(c) the low angle boundaries by misorientation angle of 0.7°-5° are shown in blue, the low angle between 5°-15° are shown in yellow, and the high angle boundaries are shown in black. The sub-boundaries in the printed structure possess a high fraction. This is considered strong evidence for activation of the extended dynamic recovery and subsequent continuous dynamic recrystallization mechanism, where recrystallization grains are formed as a result of the sub-grains formation, rotation, and coalescence.

During selective laser melting, the conditions of cyclic

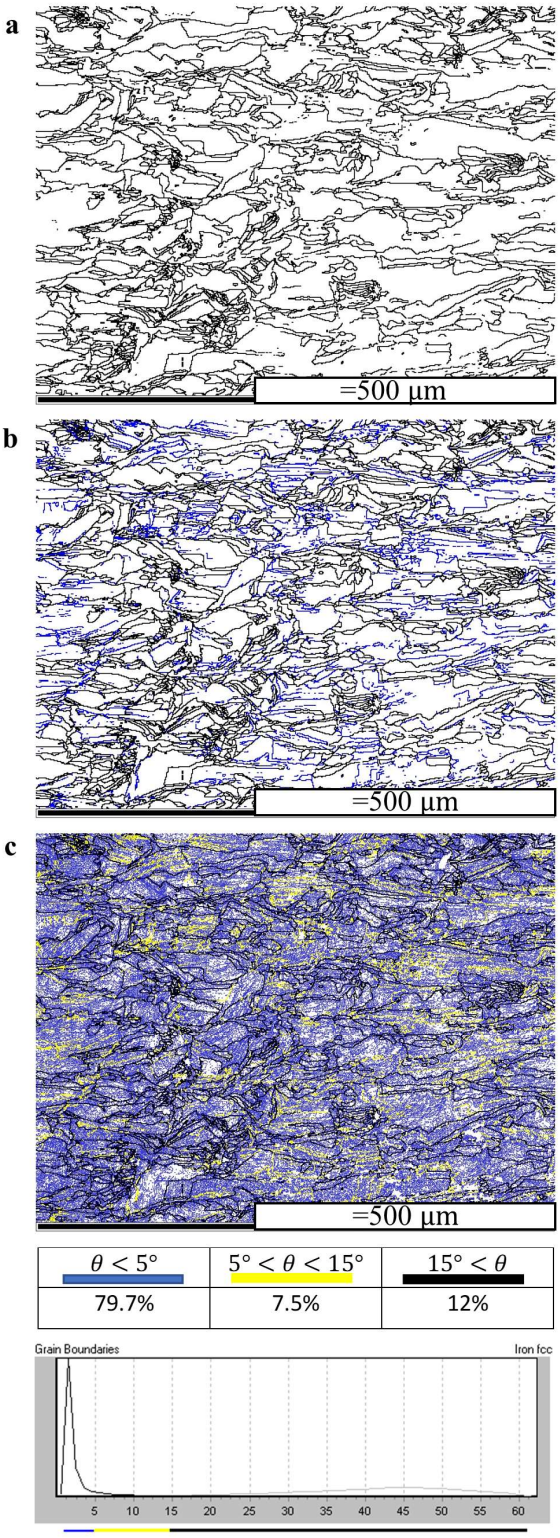

Fig. 2. The grain boundaries maps of the selective laser melted microstructure: (a) high angle grain boundaries indicated by black color (θ > 15°), (b) high angle besides low angle boundaries by misorientation of 5° < θ < 15° shown in blue, and (c) high angle (θ > 15°) and low angle boundaries shown in yellow (5° < θ < 15°) and blue (0.7° < θ< 5°).

heating and cooling are too complex, and the printed part experiences a high thermal gradient and cooling rate of about 10^3-10^8 K/s. The first thermal cycle consists of the laser melting of a layer followed by rapid cooling, which results in the development of a cellular structure during solidification. As was noted, the ratio of the thermal gradient to the growth rate (*G/R*) plays a key role in determining the characteristics of the printed microstructure. If this ratio is low, the structure is columnar, while it is possible to create a cellular structure, if it is medium. Due to the experienced rapid cooling, the *G/R* ratio is high, and it causes the formation of cellular structures in the form of circular or oval shapes or blocks [26].

The growth orientation is mainly affected by the laser energy density and the scanning strategy, which both may cause anisotropy in the mechanical properties of the printed part. In this respect, it was observed in Fig. 1 that the majority of the grains have been oriented toward <110>. A higher energy power will lead to an increase in the compatibility of the crystal growth direction with the building direction [27]. It is believed that the developed grains and cellular structure significantly influence the subsequent mechanical properties of the products. As was noted, selective laser melting can be approached as a thermomechanical processing route in which the required temperature and strain for the occurrence of dynamic recrystallization are provided. Owing to the fast cooling and heating cycles experienced during fabrication, the plastic microstrains are created through the part's structure [16]. The material expands thermally in response to local temperature changes introduced by energy from the laser beam. Heat-affected area experiences compressive stresses since the colder surrounding material acts as a constraint. During cooling, the material shrinks and tensile stresses are developed in the plastic deformation zone, leading to the occurrence of bending in the opposite direction. This has been schematically shown in Fig. 3, where N represents the printed layer and N+1, and N+2 are the next neighbor layers.

In the course of the cooling stage, the upper molten layer is initially at a higher temperature than the lower one.

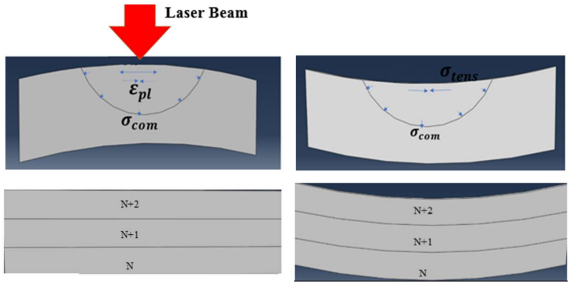

Fig. 3. General schematic of the molten pools. The micromechanisms for creation of plastic residual micro-strains during thermal and cooling cycles of the selective laser melting process.

The warmer upper layer compared to the cooler lower layer contracts to a higher extent. However, the metallurgical type connection between two layers inhibits this shrinkage. Consequently, the upper and lower layers experience tensile and compressive stresses, respectively. If the stresses exceed the compressive/tensile yield strengths of the material, the strain will be partially elastic and partially plastic [28]. The created plastic microstrain can be consumed to provide the required strain for the occurrence of partial recrystallization, and also can be remained as a residual plastic microstrain. The workpiece's or the substrate's resistance is high enough to stop plastic deformation, such as the deflection of a single layer during cooling [29].

For a detailed examination of the local plastic micro-strains distribution throughout the microstructure, the corresponding Kernel average misorientation (KAM) map is given in Fig. 4(a). The blue and red colors indicate the lowest and highest amount of local plastic strain stored within the microstructure. The red and yellow regions are attributed to the regions that have not been restored and contain residual plastic strain, and the blue and green regions may represent the presence of recovered or recrystallized grains.

As mentioned, there are two possibilities for the formation of fine equiaxed grains: (1) in the course of rapid solidification, and (2) owing to the dynamic recrystallization during additive manufacturing. In this respect, the grain orientation spread map of the selective laser melted microstructure has been illustrated in Fig. 4(b). The blue and near-blue equiaxed fine grains holding

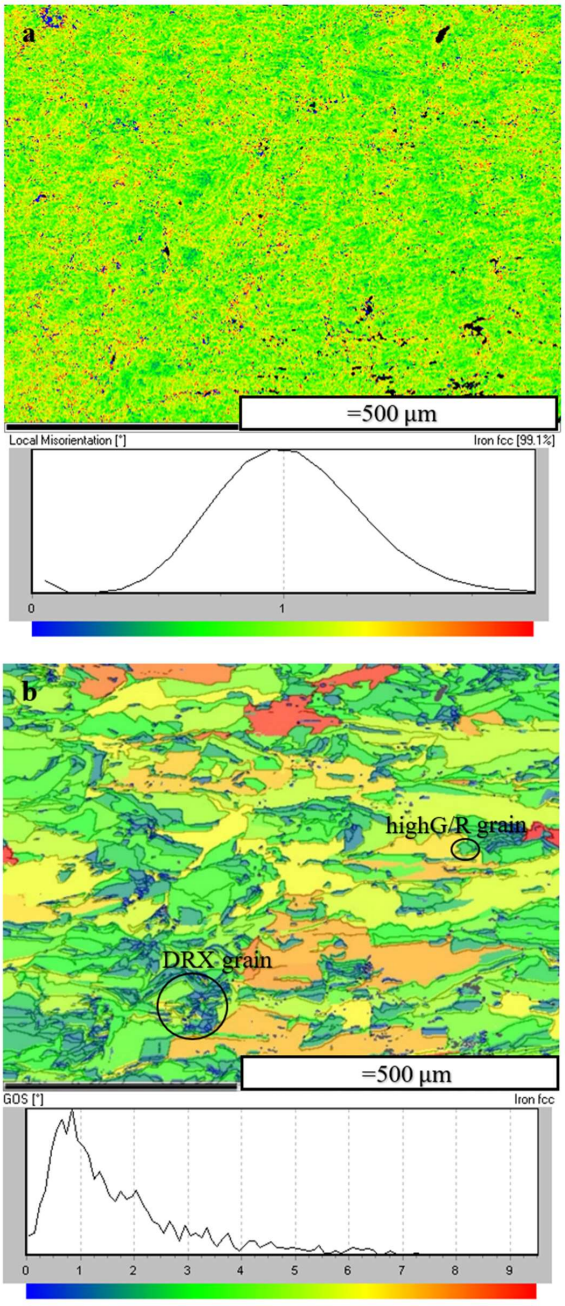

Fig. 4. (a) Kernel average misorientation (KAM) map, and (b) grain orientation spread (GOS) map of the selective laser melted microstructure.

the lowest GOS values have been formed due to the occurrence of dynamic recrystallization during the selective laser melting. The equiaxed fine grains holding higher GOS values (> 3) have been originated from the rapid solidification and local high *G/R* ratio.

As a result of the melting of a layer, some of the heat input is transferred into the previously solidified layers

due to the low thickness of the layer. In this respect, a layer may be exposed to several complicated thermal cycles. Apparently, the temperature range during selective laser melting is high enough to trigger the occurrence of restoration processes.

However, in respect of the accumulated microplastic strain, it can be calculated considering the thickness of each layer of sprayed powder (~30 µm), which becomes curved after scanning and cooling, and the average depth of the melt pools, which has been calculated to be around 19 µm according to Fig. 5(a). The experienced plastic strain is calculated through the following formula, where t is the thickness of the melt pool and t_0 is the layer of sprayed powder:

$$\varepsilon = \frac{t - t_0}{t_0} \tag{3}$$

The calculated plastic strain (~0.56) is meaningfully comparable with those (and is well higher than) critical strains of dynamic recrystallization obtained through hot compression tests. The results of hot compression testing method at 1000°C and various strain rates are given in Fig. 5(b). The flow stress reaches to the peak point and then falls down and follows a steady state regime, which well indicates the occurrence of dynamic recrystallization. The critical strain required for the occurrence of dynamic recrystallization has been calculated according to the Jonas and Poliak model [31], which is ~0.2 and considerably lower than the local plastic strain experienced in the course of additive manufacturing.

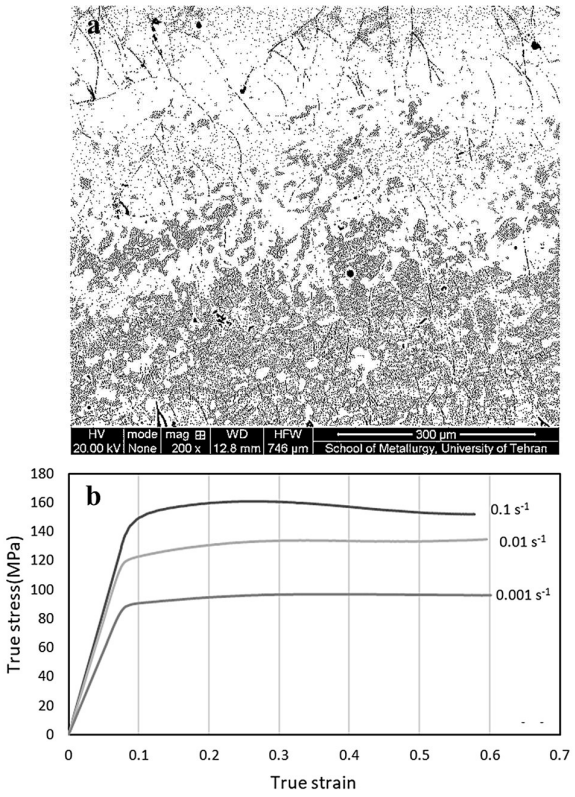

Fig. 5. (a) Scanning electron microscopy image of the selective laser melted material from lateral section, (b) the compressive true stress-true strain curves obtained at various strain rates of 0.1 s^{-1}, 0.01 s^{-1}, and 0.001 s^{-1} at 1000°C. The peak strains are depicted by red arrows.

4. Conclusion

In this research, the microstructure and microtexture of 316L stainless steel produced by selective laser melting were examined with emphasis on the probability of grain refinement in the course of the process. Selective laser melting was considered as a high temperature processing route in which the strain required for the occurrence of dynamic recrystallization could be provided. The material was prone to substructure development and extended dynamic recovery during selective laser processing, which was followed by continuous dynamic recrystallization where a considerable fraction of fine grains was formed besides the elongated grains within the melt pools. This was justified considering the experienced fast cooling and heating cycles during fabrication, where the colder surrounding material acted as constraint and provided the required plastic micro-strains for activation of dynamic recrystallization. The applied micro-strains were calculated considering the thickness of each layer which became curved after scanning and cooling. The plastic strain was meaningfully higher than critical strains of dynamic recrystallization obtained through hot compression tests.

Conflict of Interests

The authors declare that they have no known competing financial interests or personal relationships

that could have appeared to influence the work reported in this paper.

Funding

This research has not received any specific funding.

5. References

[1] W.E. Frazier, Metal additive manufacturing: a review, *Journal of Materials Engineering and Performance*, 23 (2014) 1917-1928.

[2] F. Bartolomeu, S. Faria, O. Carvalho, E. Pinto, N. Alves, F.S. Silva, G. Miranda, Predictive models for physical and mechanical properties of Ti6Al4V produced by Selective Laser Melting, *Materials Science and Engineering: A*, 663 (2016) 181-192.

[3] S.L. Sing, J. An, W.Y. Yeong, F.E. Wiria, Laser and electron-beam powder-bed additive manufacturing of metallic implants: A review on processes, materials and designs, *Journal of Orthopaedic Research*, 34(3) (2016) 369-385.

[4] A.N. Chen, J.M. Wu, K. Liu, J.Y. Chen, H. Xiao, P. Chen, C.H. Li, Y.S. Shi, High-performance ceramic parts with complex shape prepared by selective laser sintering: a review, *Advances in Applied Ceramics*, 117(2) (2018) 100-117.

[5] Y. Kok, X.P. Tan, P. Wang, M.L.S. Nai, N.H. Loh, E. Liu, S.B. Tor, Anisotropy and heterogeneity of microstructure and mechanical properties in metal additive manufacturing: A critical review, *Materials & Design*, 139 (2018) 565-586.

[6] F. Bartolomeu, M. Buciumeanu, E. Pinto, N. Alves, O. Carvalho, F.S. Silva, G. Miranda, 316L stainless steel mechanical and tribological behavior—A comparison between selective laser melting, hot pressing and conventional casting, *Additive Manufacturing*, 16 (2017) 81-89.

[7] T. DebRoy, H.L. Wei, J.S. Zuback, T. Mukherjee, J.W. Elmer, J.O. Milewski, A.M. Beese, A. Wilson-Heid, A. De, W. Zhang, Additive manufacturing of metallic components–process, structure and properties, *Progress in Materials Science*, 92 (2018) 112-224.

[8] R. Motallebi, Z. Savaedi, H. Mirzadeh, Additive manufacturing–a review of hot deformation behavior and constitutive modeling of flow stress, *Current Opinion in Solid State and Materials Science*, 26(3) (2022) 100992.

[9] L.E. Murr, S.M. Gaytan, D.A. Ramirez, E. Martinez, J. Hernandez, K.N. Amato, P.W. Shindo, F.R. Medina, R.B. Wicker, Metal fabrication by additive manufacturing using laser and electron beam melting technologies, *Journal of Materials Science & Technology*, 28(1) (2012) 1-14.

[10] O. Zinovieva, A. Zinoviev, Numerical analysis of the grain morphology and texture in 316L steel produced by selective laser melting, In: *AIP Conference Proceedings*, 2167 (2019) 020407.

[11] A. Rai, M. Markl, C. Körner, A coupled cellular automaton–lattice Boltzmann model for grain structure simulation during additive manufacturing, *Computational Materials Science*, 124 (2016) 37-48.

[12] C. Herriott, X. Li, N. Kouraytem, V. Tari, W. Tan, B. Anglin, A.D. Rollett, A.D. Spear, A multi-scale, multi-physics modeling framework to predict spatial variation of properties in additive-manufactured metals, *Modelling and Simulation in Materials Science and Engineering*, 27(2) (2019) 025009.

[13] R. Shi, S.A. Khairallah, T.T. Roehling, T.W. Heo, J.T. McKeown, M.J. Matthews, Microstructural control in metal laser powder bed fusion additive manufacturing using laser beam shaping strategy, *Acta Materialia*, 184 (2020) 284-305.

[14] O. Zinovieva, A. Zinoviev, V. Ploshikhin, Three-dimensional modeling of the microstructure evolution during metal additive manufacturing, *Computational Materials Science*, 141 (2018) 207-220.

[15] A. Baumard, D. Ayrault, O. Fandeur, C. Bordreuil, F. Deschaux-Beaume, Numerical prediction of grain structure formation during laser powder bed fusion of 316 L stainless steel, *Materials & Design*, 199 (2021) 109434.

[16] K.M. Bertsch, G.M. De Bellefon, B. Kuehl, D.J. Thoma, Origin of dislocation structures in an additively manufactured austenitic stainless steel 316L, *Acta Materialia*, 199 (2020) 19-33.

[17] N. Chen, G. Ma, W. Zhu, A. Godfrey, Z. Shen, G. Wu, X. Huang, Enhancement of an additive-manufactured austenitic stainless steel by post-manufacture heat-treatment, *Materials Science and Engineering: A*, 759 (2019) 65-69.

[18] P. Bajaj, A. Hariharan, A. Kini, P. Kürnsteiner, D. Raabe, E.A. Jägle, Steels in additive manufacturing: a review of their microstructure and properties, *Materials Science and Engineering: A*, 772 (2020) 138633.

[19] O.O. Salman, C. Gammer, A.K. Chaubey, J. Eckert, S. Scudino, Effect of heat treatment on microstructure and mechanical properties of 316L steel synthesized by selective laser melting, *Materials Science and Engineering: A*, 748 (2019) 205-212.

[20] S. Waqar, J. Liu, Q. Sun, K. Guo, J. Sun, Effect of post-heat treatment cooling on microstructure and mechanical properties of selective laser melting

manufactured austenitic 316L stainless steel, *Rapid Prototyping Journal*, 26(10) (2020) 1739-1749.

[21] M. Güden, S. Enser, M. Bayhan, A. Taşdemirci, H. Yavaş, The strain rate sensitive flow stresses and constitutive equations of a selective-laser-melt and an annealed-rolled 316L stainless steel: a comparative study, *Materials Science and Engineering: A*, 838 (2022) 142743.

[22] S.P. Kumar, V. Chakkravarthy, A. Mahalingam, R. Rajeshshyam, N. Sriraman, P. Marimuthu, R.L. Narayan, P.D. Babu, Investigation of crystallographic orientation and mechanical behaviour in laser-welded stainless steel 316L additive components, *Transactions of the Indian Institute of Metals*, 76(2) (2023) 527-535.

[23] M. Fousová, D. Dvorský, A. Michalcová, D. Vojtěch, Changes in the microstructure and mechanical properties of additively manufactured AlSi10Mg alloy after exposure to elevated temperatures, *Materials Characterization*, 137 (2018) 119-126.

[24] Y. Li, D. Gu, Parametric analysis of thermal behavior during selective laser melting additive manufacturing of aluminum alloy powder, *Materials & Design*, 63 (2014) 856-867.

[25] K. Saeidi, X. Gao, Y. Zhong, Z.J. Shen, Hardened austenite steel with columnar sub-grain structure formed by laser melting, *Materials Science and Engineering: A*, 625 (2015) 221-229.

[26] J. Song, Y. Chew, G. Bi, X. Yao, B. Zhang, J. Bai, S.K. Moon, Numerical and experimental study of laser aided additive manufacturing for melt-pool profile and grain orientation analysis, *Materials & Design*, 137 (2018) 286-297.

[27] J. Suryawanshi, K.G. Prashanth, U. Ramamurty, Mechanical behavior of selective laser melted 316L stainless steel, *Materials Science and Engineering: A*, 696 (2017) 113-121.

[28] A. Ahmadi, R. Mirzaeifar, N.S. Moghaddam, A.S. Turabi, H.E. Karaca, M. Elahinia, Effect of manufacturing parameters on mechanical properties of 316L stainless steel parts fabricated by selective laser melting: a computational framework, *Materials & Design*, 112 (2016) 328-338.

[29] J.P. Kruth, J. Deckers, E. Yasa, R. Wauthlé, Assessing and comparing influencing factors of residual stresses in selective laser melting using a novel analysis method, *Proceedings of the Institution of Mechanical Engineers, Part B: Journal of Engineering Manufacture*, 226(6) (2012) 980-991.

[30] T. Simson, A. Emmel, A. Dwars, J. Böhm, Residual stress measurements on AISI 316L samples manufactured by selective laser melting, *Additive Manufacturing*, 17 (2017) 183-189.

[31] H.E. Sabzi, X.H. Li, C. Zhang, H. Fu, D. San-Martín, P.E.J. Rivera-Díaz-del-Castillo, Deformation twinning-induced dynamic recrystallization during laser powder bed fusion, *Scripta Materialia*, 207 (2022) 114307.

[32] E.I. Poliak, J. Jonas, A one-parameter approach to determining the critical conditions for the initiation of dynamic recrystallization, *Acta Materialia*, 44(1) (1996) 127-136.